Supplemental Information

Overcoming photovoltage deficit via natural amino acid passivation for efficient perovskite solar cells and modules

Jinlong Hu,[1] Xin Xu,[2] Yijun Chen,[1] Shaohang Wu,[1] Zhen Wang,[1] Yousheng Wang,[1] Xiaofang Jiang,[3] Boyuan Cai,[4] Tingting Shi,[2] Christoph J. Brabec[5,6], Yaohua Mai[1*], and Fei Guo[1,7*]*

[1]Institute of New Energy Technology, College of Information Science and Technology, Jinan University, Guangzhou 510632, China

[2]Siyuan Laboratory Guangzhou Key Laboratory of Vacuum Coating Technologies and New Energy Materials Department of Physics, Jinan University, Guangzhou 510632, P. R. China

[3]State Key laboratory of Optic Information Physics and Technologies, School of Physics and Telecommunication Engineering, South China Normal University, Guangzhou 510006, China

[4]Centre for Artificial-Intelligence Nanophotonics School of Optical-Electrical and Computer Engineering University of Shanghai for Science and Technology, Shanghai, 200000, China

[5]Institute of Materials for Electronics and Energy Technology (i-MEET), Friedrich-AlexanderUniversity Erlangen-Nürnberg, Martensstrasse 7, 91058 Erlangen, Germany.

[6]Forschungszentrum Jülich, Helmholtz-Institute Erlangen-Nuremberg for Renewable Energies (IEK 11), Immerwahrstr. 2, 91058 Erlangen, Germany

[7]Key Laboratory of Advanced Material Processing & Mold (Ministry of Education), Zhengzhou University, Zhengzhou, 450002, China

e-mail: ttshi@jnu.edu.cn; yaohuamai@jnu.edu.cn; fei.guo@jnu.edu.cn

Experimental Section

Materials: Methylammonium iodide (MAI), Lead iodide (PbI$_2$, 99.9985%), and Poly[bis(4-phenyl) (2,4,6-trimethylphenyl) amine] (PTAA) were purchased from Xi'an p-OLED Co. (China). Bathocuproine (BCP) and PC$_{61}$BM were purchased from Lumtec. Glycine, glutamic acid, proline, and arginine were purchased from Bide Pharmatech Ltd. Lysine, histidine, serine, threonine, phenylalanine and aspartic acid were purchased from Tokyo Chemical Industry (TCI). All the solvents were purchased from Sigma-Aldrich. All the chemicals were used as received without further purification.

Blade Deposition of Perovskite Films: The MAPbI$_3$ precursor solution was prepared by dissolving 1 mol equimolar ratio of MAI and PbI$_2$with 1 mg NAAs (Gly, Glu, Pro, Arg, etc.) in mixed solvent of DMSO and DMF (volume ratio 200 uL:800 uL). After stirring for 1 h at room temperature, the precursor solution with concentration of 1 mol/L was filtered and transferred into nitrogen-filled glovebox. Blade-coating of the perovskite precursor films was performed on a commercial-blade coater (ZAA2300.H from ZEHNTNER) using a ZUA 2000.100 blade (from ZEHNTNER) at room temperature in nitrogen-filled glovebox. 20 µL precursor solution was used for blade deposition on substrate with a dimension of 2.5 $\varnothing$ 2.5 cm^2. The gap for solution load between the substrate and blade was fixed at 200 µm. Once the precursor solution was spread onto the substrate by blade-coating, the liquid precursor film was transferred into a vacuum chamber, which was pumped to 1000 Pa in 15 s and stayed at the pressure for 90 second. Subsequently, the film was brought out of the vacuum chamber and annealed at 100 °C for 10 min to fully crystallize the film.

Devices Fabrication: The pre-patterned indium tin oxide (ITO) coated glass (OPV Tech Co., Ltd.) was sequentially cleaned by sonicating the substrates in acetone and isopropanol for 10 min each. A PTAA hole-transporting layer was spin-coated from 5 mg mL^{-1} CB solution on ITO substrate at 5000 rpm for 30 sec. The film was then annealed at 120 °C for 10 min in ambient air. The substrate was then transferred to a

nitrogen-filled glovebox after it cooled down to room temperature. On top of perovskite film, the electro-transporting layer $PC_{61}BM$ (20 mg mL^{-1} in chlorobenzene) and the interfacial layer BCP (2.5 mg mL^{-1} in isopropanol) was successively deposited by spin coating at 2000 rpm for 30 sec and 5000 rpm for 30 sec, respectively. Finally, 120 nm Ag layer was deposited by thermal evaporation. The active areas of the solar cells are 0.09 cm^2 for the small-size ($MAPbI_3$) devices, which are determined by the overlapping between the top Ag and bottom ITO electrode. All the devices for performance and stability evaluation were tested without encapsulation.

Materials Characterizations: The morphology and microstructure of the thin films were investigated using field emission scanning electron microscopy (SEM, FEI Apreo LoVac). The crystal structure was characterized by Bruker D8 Advance X-ray diffractometer with CuKα radiation operated at 40 kV and 40 mA. X-ray photoelectron spectroscopy (XPS) experiments were also carried out on an ESCALab250Xi electron spectrometer (Thermo Fisher) using Al Kα radiation. Attenuated total reflection Fourier transform infrared (ATR-FTIR) spectra were acquired on an FTIR spectrometer (Alpha-P, Bruker Optics, Billerica, MA, U.S.A.) in transmission mode. The samples for ATR-FTIR measurements were prepared through scratching thin films of $MAPbI_3$ and Arg-modified $MAPbI_3$ from ITO (indium tin oxide) substrates. High resolution transmission electron microscope (HRTEM) was performed on JEOL JEM- 2100F with acceleration voltage of 200 KV. We scraped the Arg-modified $MAPbI_3$ thin films from glass, and ultrasonically dispersed in anhydrous chlorobenzene solvent. Subsequently, 10 µL of the as-prepared solution were dropped on copper mesh with microgrid for the HRTEM measurement. Time resolved PL experiments were performed with a spectrophotometer (Gilden Photonics) using a pulsed source at 480 nm (Ps diode lasers BDS-SM). The time-resolved signals were recorded by a time correlated single photon counting detection technique with a time resolution of 1 ns. The current density-voltage (J-V) characteristics and steady-state output of the all solar cells were measured using a Keithley 2400 source meter. The illumination was provided by a Newport Oriel 92192 solar simulator with an

AM1.5G filter, operating at 100 mW cm^{-2}, which was calibrated by a standard silicon solar cell from Newport. The external quantum efficiency (EQE) was taken using a QE-R instrument from Enlitech.

Calculation Methodology: In this paper, the theoretical calculations were performed by density function (DFT) methods. DFT calculations were performed under exchange correlation function of generalized gradient approximation (GGA)[1] with Perdew, Burke, and Ernzerhof (PBE). The calculations for surface passivation were performed by VASP[2] code with the projector augmented wave method (PAW)[3]. The Kohn-Sham equation is solved by a plane wave basis set with a cutoff energy of 400 eV, and the Brillouin zone samples a 2×2×1 mesh centered at Γ point. Atoms are fully relaxed until the Hellmann-Feynman forces on them are within 0.05 eV/A. The calculations of electrostatic potential (ESP) were conducted on the Guassian 09 program by using B3PW91 and the all-electron double-ξ valence basis sets of 3-21G*. Geometry optimizations of amino acids were performed with default spin mode.

1. S. Grimme, S. Ehrlich and L. Goerigk, J Comput Chem, 2011, 32, 1456-1465.
2. G. Kresse and J. Furthmüller, Physical Review B, 1996, 54, 11169-11186.
3. G. Kresse and D. Joubert, Physical Review B, 1999, 59, 1758-1775.
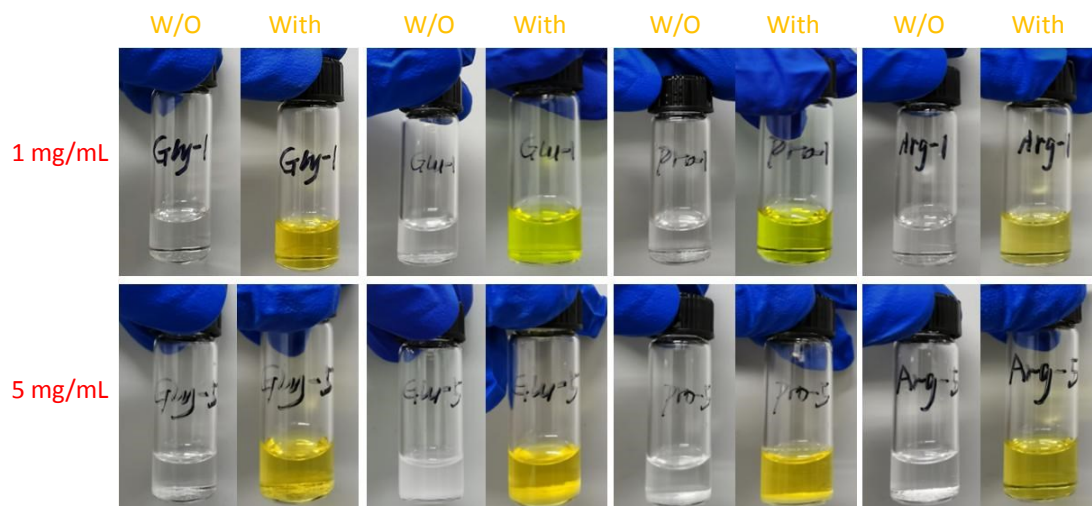
Figure S1. Solubility test of the various NAAs in DMF with and without (W/O) addition of PbI$_2$. The concentration of NAAs in the top row and the bottom row is 1 and 5 mg/mL, respectively.
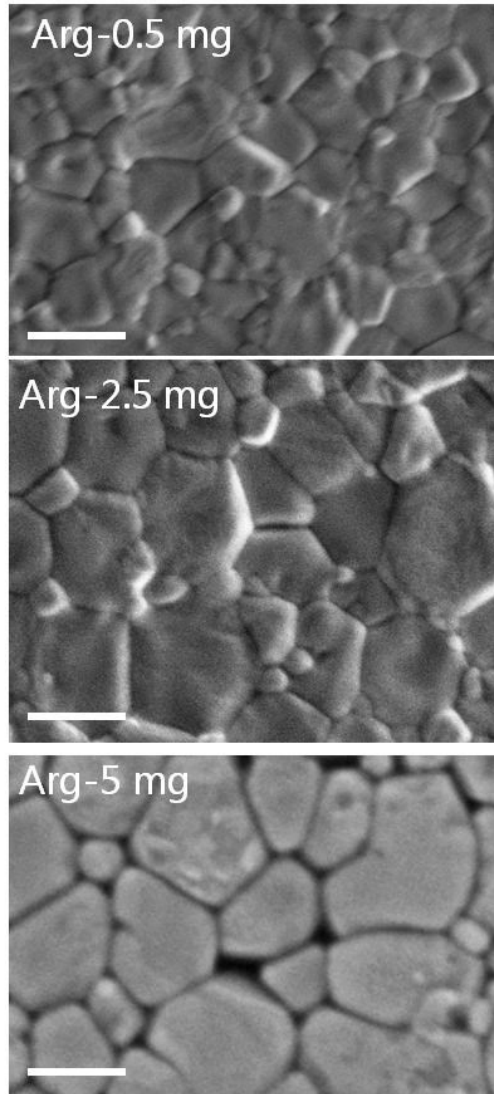
Figure S2. Top-view SEM images of the perovskite films prepared with incorporation of 0.5, 2.5 and 5 mg/mL Arg. The scale bars are 1 μm.
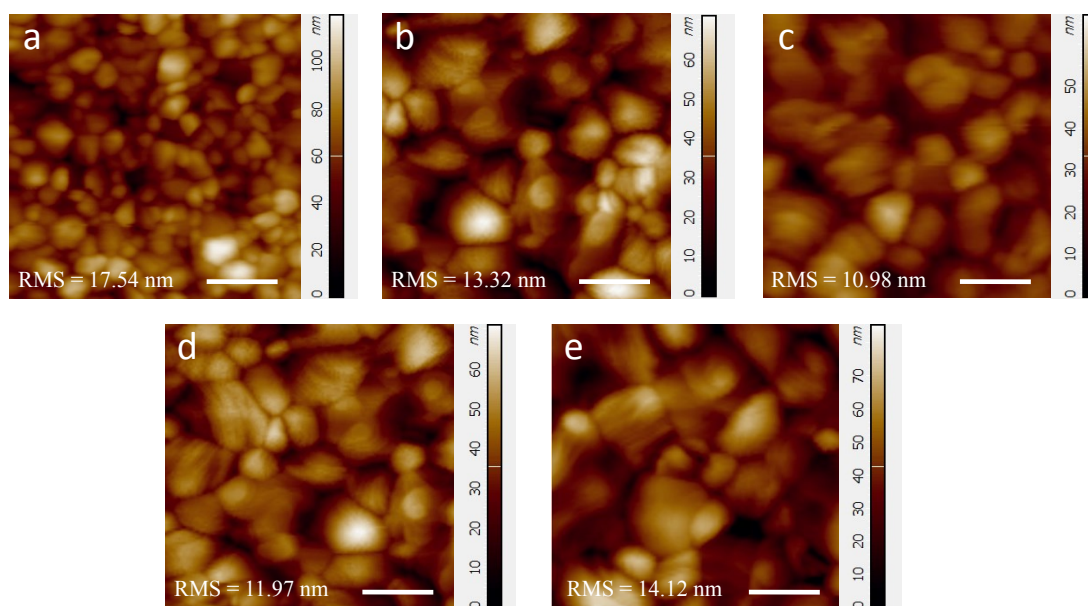
Figure S3. AFM images of the (a) pristine, (b) Gly-, (c) Glu-, (d) Pro- and (e) Arg-modified thin films. The scale bar is 1 um.
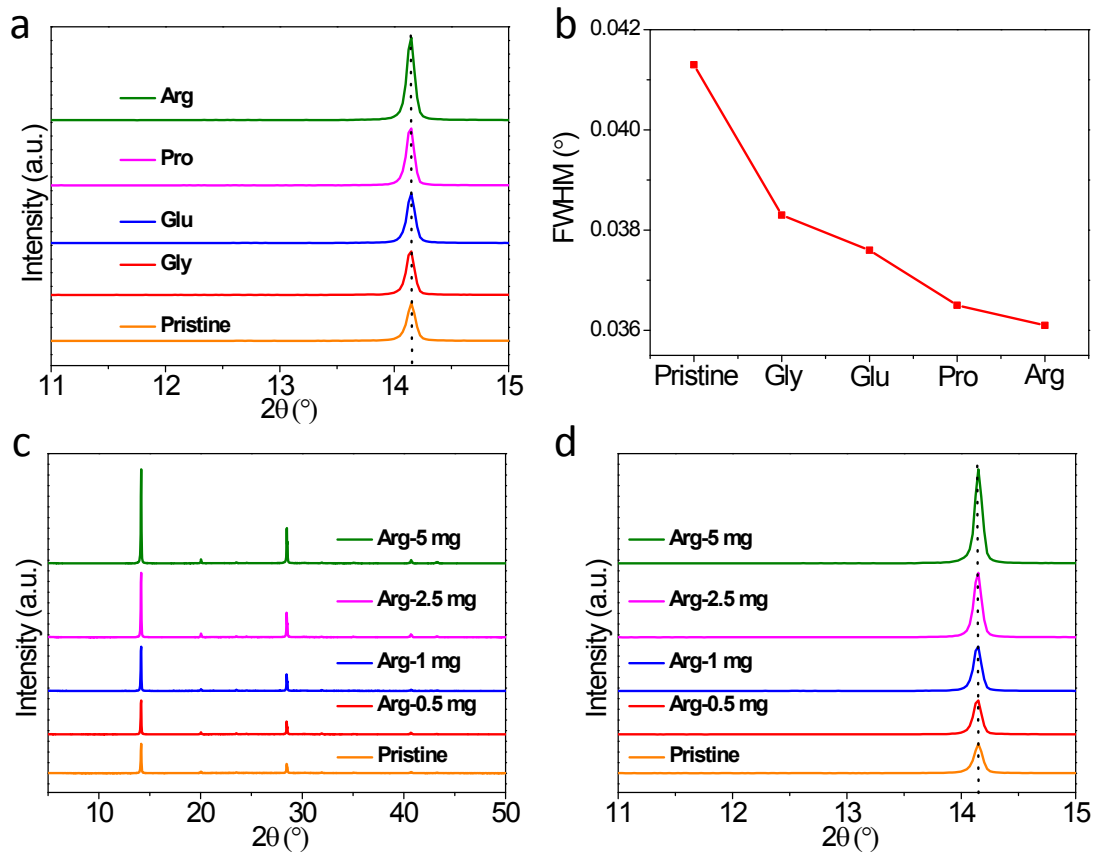
Figure S4. (a) Zoom-in XRD spectra of the MAPbI$_3$ perovskite films processed without and with addition of different NAAs. (b) FWHM of the (110) peak of the films processed without and with addition of different NAAs. (c) XRD spectra of the MAPbI$_3$ perovskite films processed with different concentration of Arg. (d) Zoom-in XRD spectra of the films processed processed with different concentration of Arg.
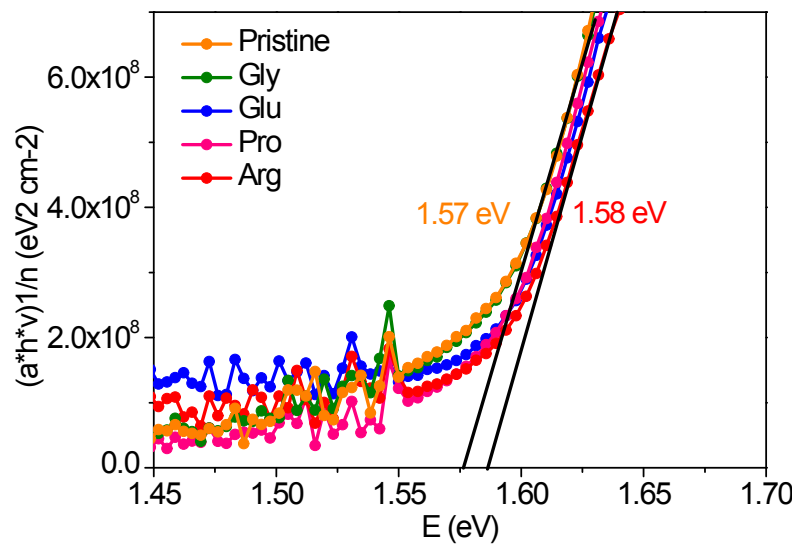
Figure S5. Tauc plots of $(ahv)^2$ vs. hv of the perovskite films processed without and with addition of different NAAs.
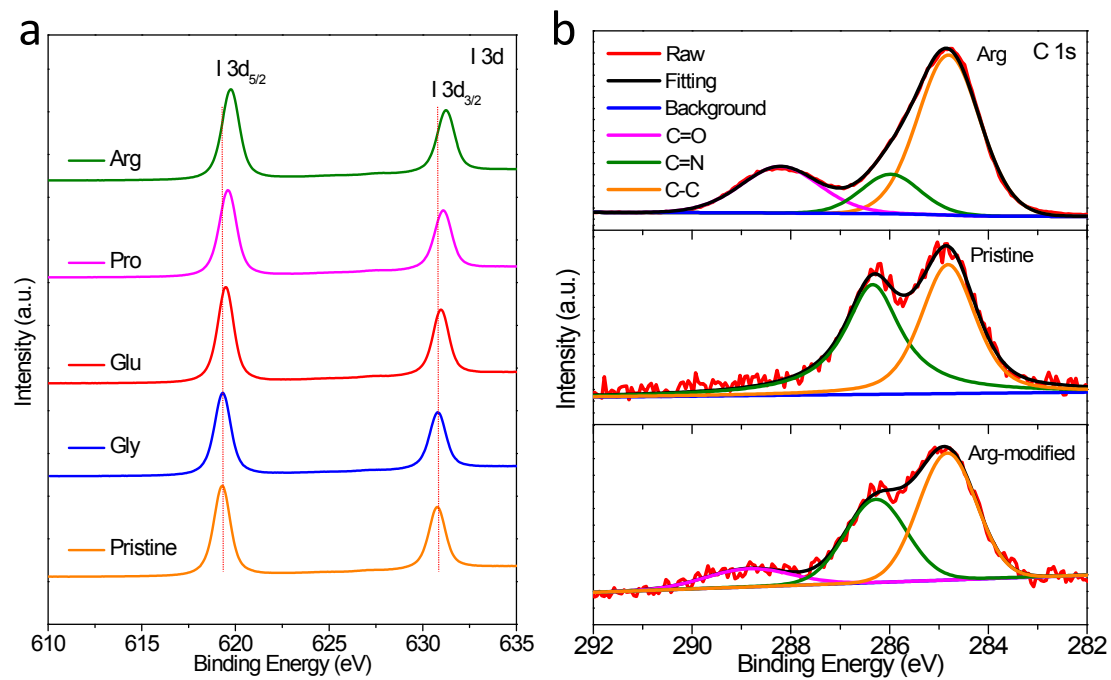
Figure S6. (a) High-resolution I 3d spectra of perovskite films without and with various NAAs modification. (b) XPS spectra of C 1s for the Arg powder, pristine and Arg-modified perovskite films.
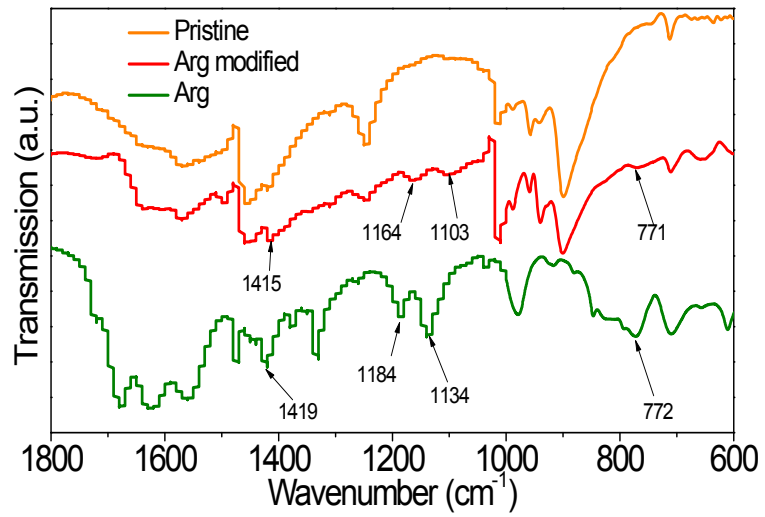
Figure S7. Attenuated total reflection Fourier transform infrared (ATR-FTIR) spectra of Arg, pristine MAPbI$_3$ and Arg-modified MAPbI$_3$ powders.
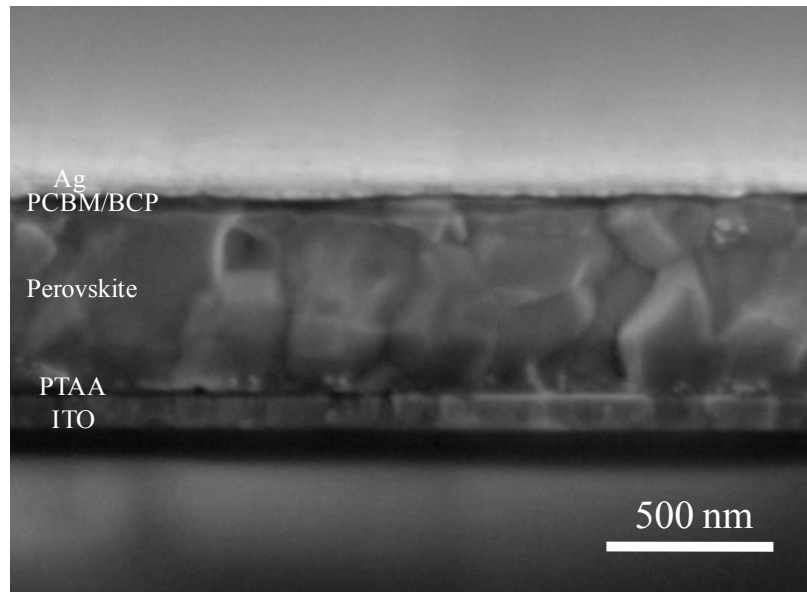
Figure S8. Cross-sectional SEM image of the Arg-modified solar cell.
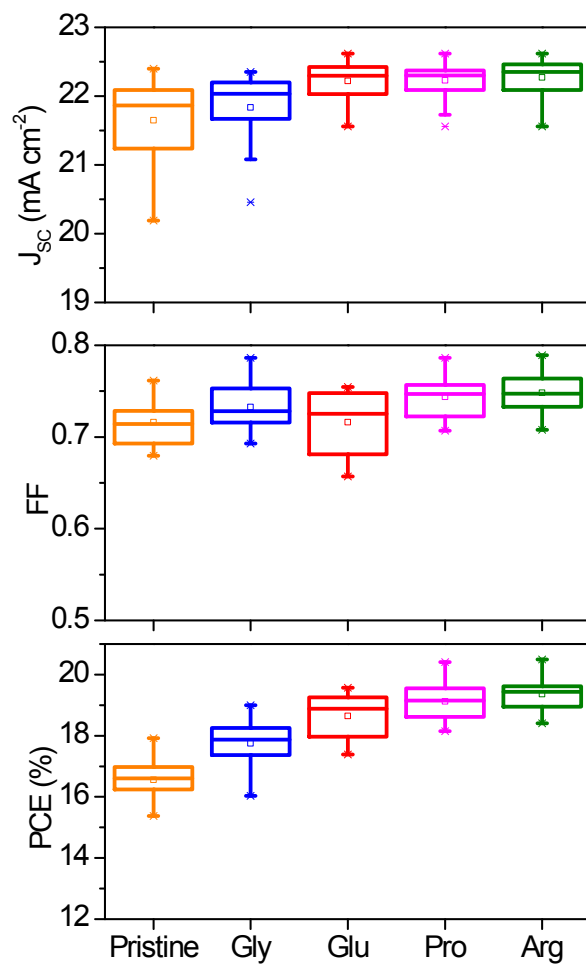
Figure S9. Statistic distributions of the J_{SC}, FF and PCE of the pristine device and the NAAs-modified devices.
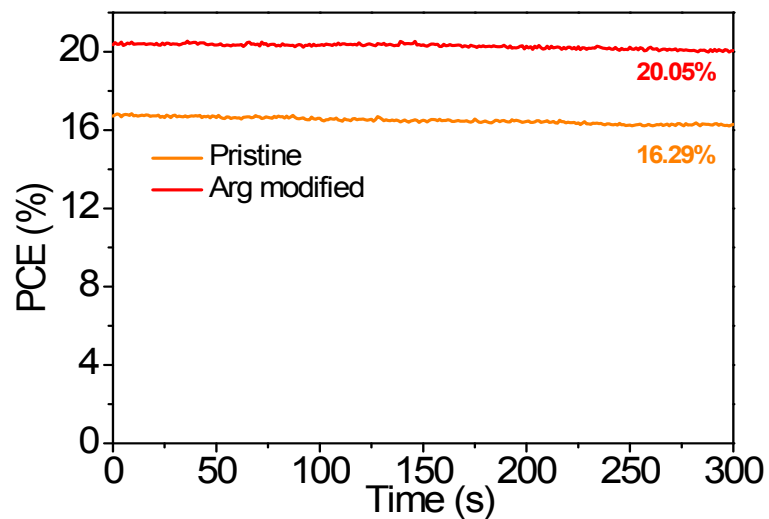
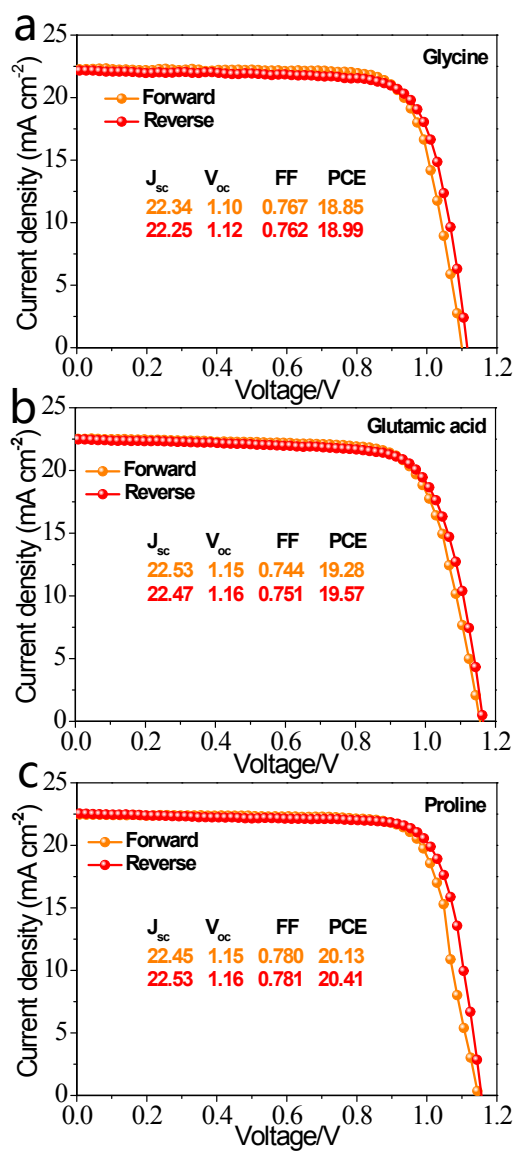**Figure S10.** The stabilized power output of the pristine and Arg-modified MAPbI$_3$ cells monitored at the maximum power point for 300 seconds.

Figure S11. *J-V* curves of the perovskite solar devices measured from both forward and reverse scan directions: (a), (b), and (c) are the *J-V* curves of the devices with modification of glycine, glumatic acid, and proline, respectively. The concentration of the respective NAAs is 1 mg mL^{-1}.
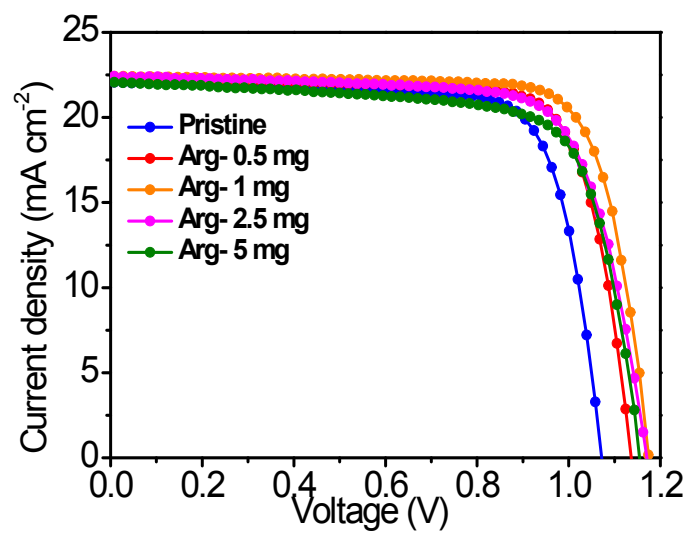
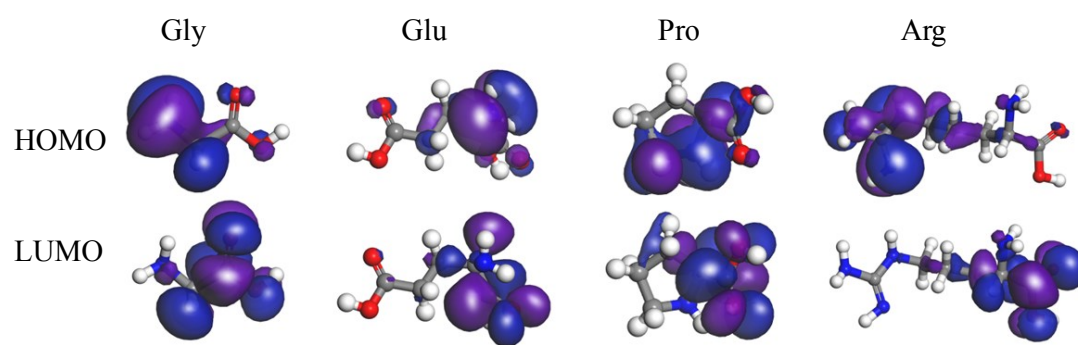**Figure S12.** J-V characteristics of the MAPbI$_3$ cells passivated with different amounts of Arg.

Figure S13. Calculated electron distribution (HOMO and LUMO) of the Gly, Glu, Pro and Arg molecules.
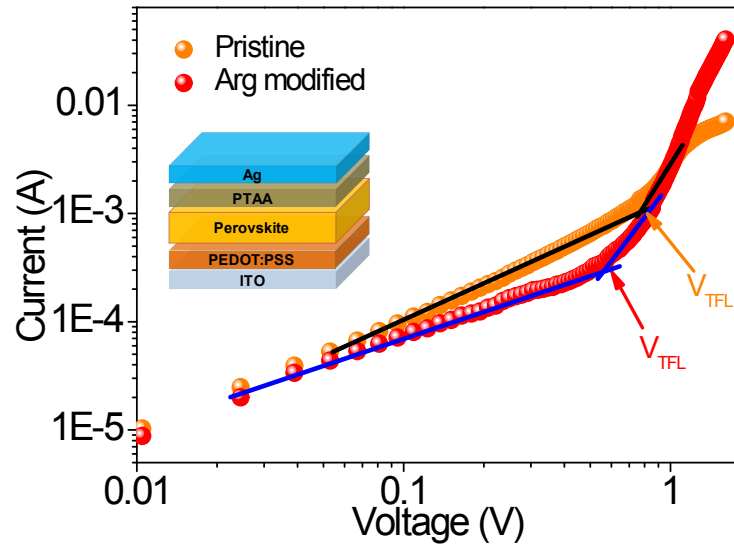
Figure S14. I-V logarithm curves in the dark for the pristine device and the Arg-modified device.
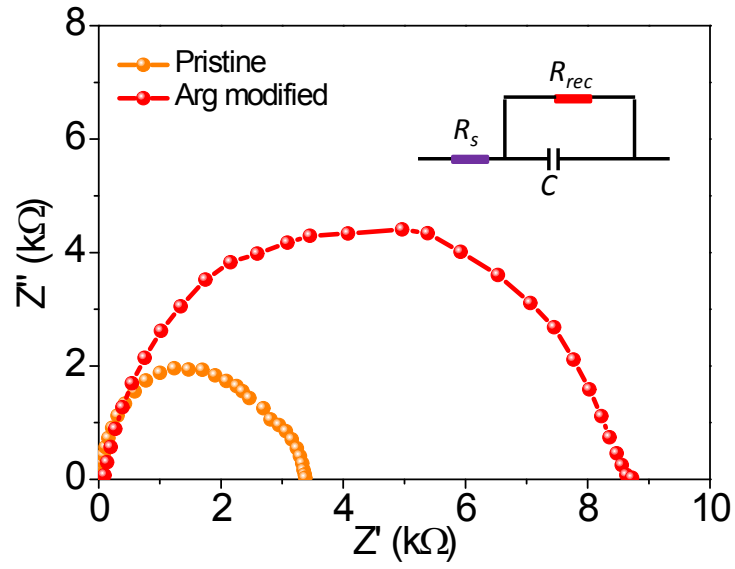
Figure S15. Nyquist plots of the pristine device and the Arg-modified device measured at a voltage of 0.7 V in dark. Inset shows the equivalent circuit model, where C, R_s, and R_{rec} represent junction capacitance, series resistance and recombination resistance, respectively.
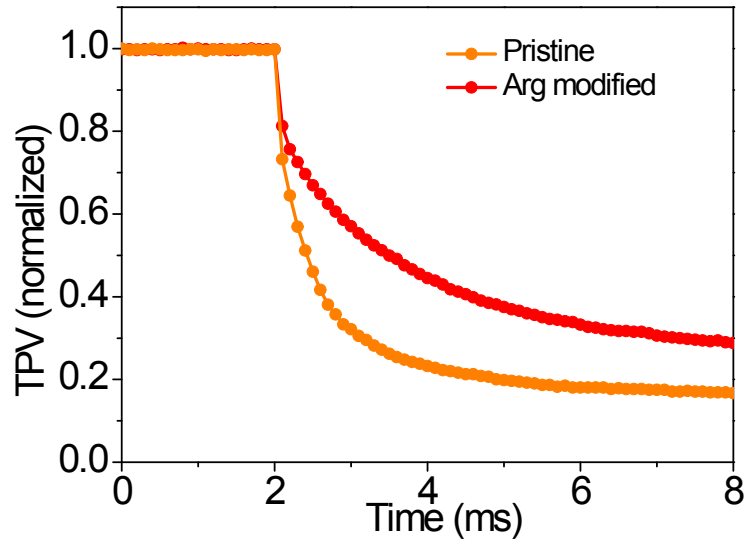
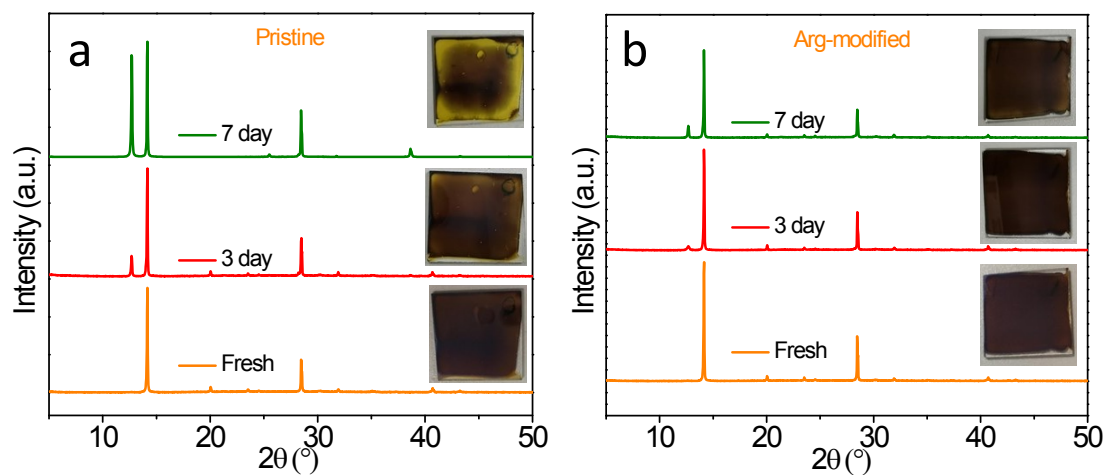**Figure S16.** V_{OC} decay as the function of time of the pristine cell and Arg-modified MAPbI$_3$ cell.

Figure S17. XRD spectra evolution of the pristine (a) and the Arg-modified (b) perovskite films stored at ambient air with a RH of 50 ± 10% for a week (a and b). Photos in the insets display the color change of the films.
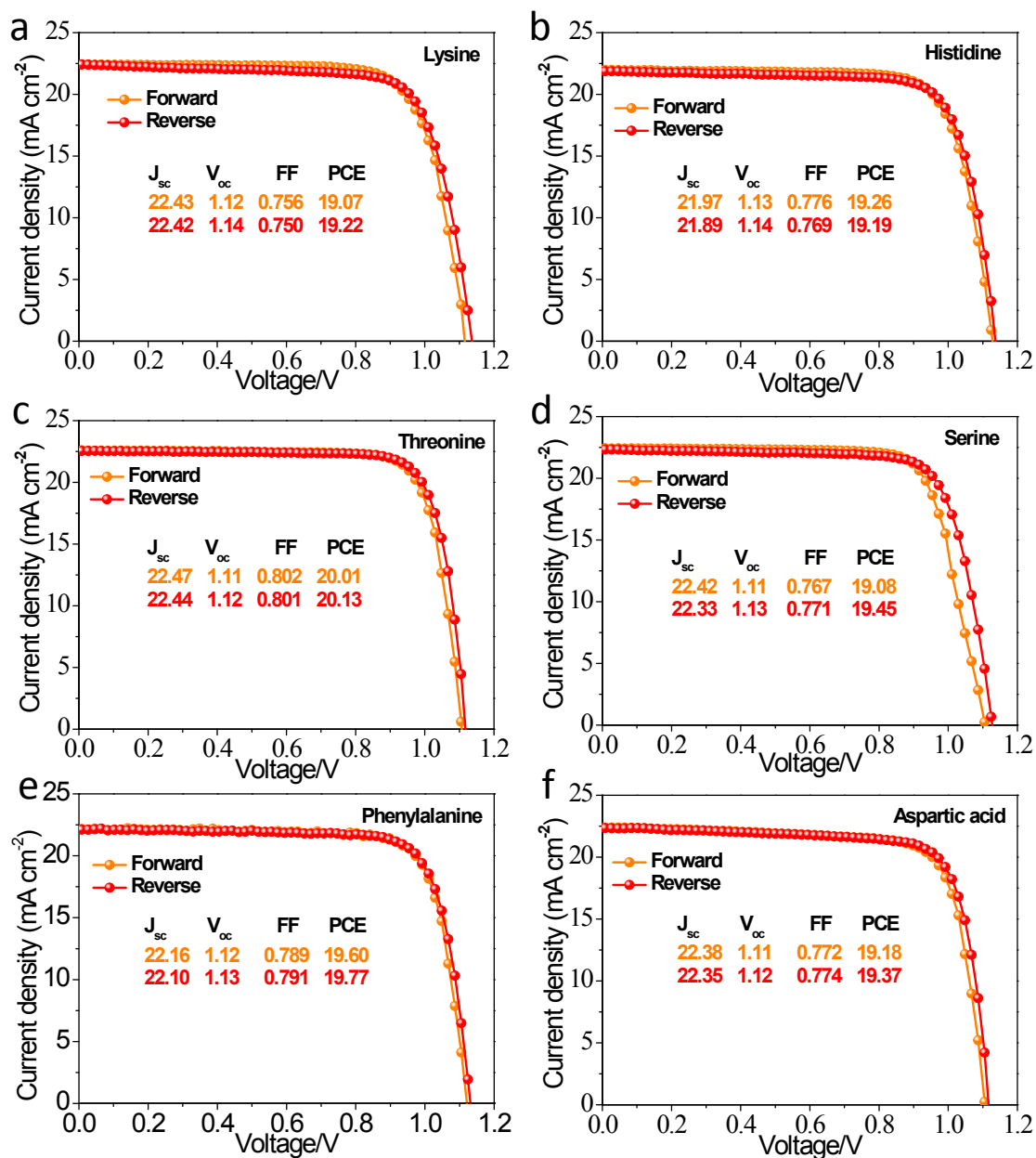
Figure S18. *J-V* curves of the perovskite solar devices measured from both forward and reverse scan directions: (a), (b), (c), (d), (e) and (f) are the *J-V* curves of the devices passivated with lysine, histidine, threonine, serine, phenylalanine and aspartic acid, respectively. The concentration of the respective NAA is 1 mg mL^{-1}.

Table S1. A summary of the device performances of the MAPbI$_3$ solar cells collected from the literature.

PCE (%)	Active area (cm^2)	V$_{OC}$ (V)	J$_{SC}$ (mA cm^{-2})	Note	Reference
20.4%	0.06	1.14	23.48	Spin-coating	Adv. Mater. **2020,** 32, 1905661
19.87%	0.09	1.11	22.38	Spin-coating	J. Mater. Chem. A **2018,** 6, 6255
20.1%	0.16	1.156	22.7	Spin-coating	J. Am. Chem. Soc. **2020,** 142, 2364
20.78%	0.16	1.12	23.01	Spin-casting	Nano Energy **2020, 6**7, 104229
20.84%	0.1	1.14	22.08	Spin-coating	Adv. Funct. Mater. **2019,** 29, 1901026
20.28%	0.09	1.16	22.61	Spin-coating	Adv. Energy Mater. **2019,** 9, 1803573
19.28%	0.09	1.10	22.88	Spin-coating	Adv. Mater. **2018,** 30, 1706576
20.4%	0.09	1.14	22.60	Spin-coating	Adv. Mater. **2019,** 31, 1901519
18%	0.09	1.06	22.3	Spin-coating	Adv. Funct. Mater. **2018,** 28, 1801654
20.63%	0.096	1.12	23.46	Spin-coating	ACS Energy Lett. **2019,** 4, 2646
17.54%	0.09	1.08	22.68	Blade-coating	ACS Energy Lett. **2018,** 3, 1078
21.7%	0.08	1.18	22.5	Blade-coating	Sci. Adv. **2019,** 5, eaav8925
20.14%	0.09	1.19	22.36	Blade-coating	Adv. Energy Mater. **2020,**10, 200173
20.49%	**0.09**	**1.17**	**22.40**	**Blade-coating**	**This work**

Table S2. Photovoltaic parameters of the planar p-i-n structure perovskite solar cells with different concentrations of Arg treatment.

Active layer	J_{SC} (mA cm^{-2})	V_{OC} (V)	FF (%)	PCE (%)
MAPbI$_3$	22.06	1.07	75.9	17.91
MAPbI$_3$/Arg (0.5 mg/ml)	22.32	1.14	76.7	19.52
MAPbI$_3$/Arg (1 mg/ml)	22.40	1.17	78.2	20.49
MAPbI$_3$/Arg (2.5 mg/ml)	22.42	1.17	74.5	19.54
MAPbI$_3$/Arg (5 mg/ml)	21.98	1.15	73.1	18.47
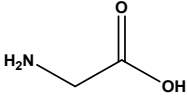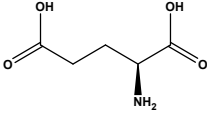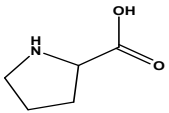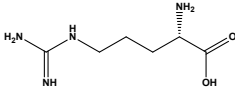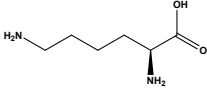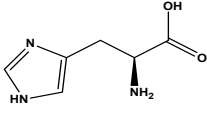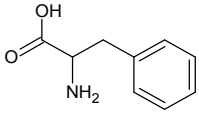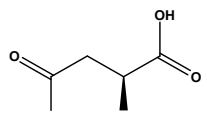
Table S3. The PL decay time (τ) parameters obtained from the exponential fitting curves for the pristine and various NAAs modified perovskite devices.
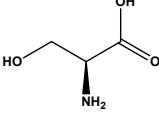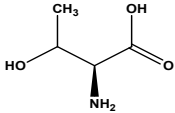
/	τ_1 (ns)	A_1	τ_2 (ns)	A_2	τ_{avg} (ns)
Pristine	127.7	0.62	416.4	0.90	298.6
Gly-modified	137.8	0.42	443.6	0.92	325.3
Glu-modified	131.8	0.32	502.5	0.92	406.8
Pro-modified	123.8	0.40	514.2	0.94	397.6
Arg-modified	270.2	0.45	667.5	0.71	513.4

Table S4. The calculated total energies, adsorption energies, N-Pb bonding lengths and barder charge of different models, including defective $MAPbI_3/Pb_I$ perovskite, $Gly/MAPbI_3$ system and $Arg/MAPbI_3$ system.

Structural Configurations	Total Energy (eV)	Adsorption Energy (eV)	N-Pb bonding length (Å)	Bader Charge
$MAPbI_3$ w/ Pb_I	-961.14	1.14	76.7	3.89
$Gly/MAPbI_3$	-1020.01	-0.66	2.66	3.66
w/ high density	-1027.26			3.24
$Arg/MAPbI_3$	-1114.84	-0.71	2.44	3.65
w/ high density	-1121.86			3.19

Table S5. The photovoltaic parameters of the best-performing MAPbI$_3$ solar cells passivated with various NAAs. The concentration of the respective NAA is 1 mg mL^{-1}.

Additives	Abbreviations	Structural formula	J_{SC} (mA cm^{-2})	V_{OC} (V)	FF (%)	PCE (%)
Pristine	-	-	22.06	1.07	75.9	17.91
Glycine	Gly		22.25	1.12	76.2	18.99
Glutamic acid	Glu		22.47	1.16	75.1	19.57
Proline	Pro		22.53	1.16	78.1	20.41
Arginine	Arg		22.40	1.17	78.2	20.49
Lysine	Lys		22.42	1.14	75.0	19.22
Histidine	His		21.97	1.13	77.6	19.26
Serine	Ser		22.33	1.13	77.1	19.45
Threonine	Thr		22.44	1.12	80.1	20.13
Phenylalanine	Phe		22.10	1.13	79.1	19.77
Aspartic acid	Asp		22.35	1.12	77.4	19.37